International Journal of Solids and Structures 167 (2019) 1–13

Contents lists available at ScienceDirect

International Journal of Solids and Structures

journal homepage: www.elsevier.com/locate/ijsolstr

On the applicability of replacement relations to tetrahedron-like inhomogeneities

A. Markov*, A. Trofimov, S. Abaimov, I. Akhatov

Center for Design, Manufacturing, and Materials, Skolkovo Institute of Science and Technology, Skolkovo 121205 Russia

ARTICLE INFO

Article history:
Received 11 December 2018
Revised 25 February 2019
Available online 27 February 2019

Keywords:
Inhomogeneities
Micromechanics
Tetrahedral inclusions
Finite element method
Volume integral equation
Gaussian approximation
Compliance contribution tensor
Replacement relations

ABSTRACT

In this paper, we consider the problem of elastic materials containing tetrahedron-like inhomogeneities with spherical polygons as faces. The overall properties are expressed in terms of compliance contribution tensors calculated for inhomogeneities of different face curvature and elastic properties. The calculations were performed by two numerical techniques: Finite Element Method (FEM) and Volume Integral Equation Method (VIEM) combined with mesh-free discretization by Gaussian approximating functions. Consistency of the results obtained by these methods is observed in most cases. Applicability of replacement relations that predict the contribution to the overall elastic properties of inhomogeneities with different elastic properties, but the same shape, was analyzed. The replacement relations provide considerably good approximation for "soft" inclusions (Young's modulus lower than the matrix') only, in certain cases wrong approximation trends were observed. It was possible to propose an adjustment tensor for the replacement relations which components depend linearly on the face curvature.

1. Introduction

Inhomogeneities of tetrahedron-like shapes are commonly observed in natural and artificial materials. For example, tetrahedral (Fig. 1a) or concave tetrahedral (Fig. 1b) nanocrystals are widely used as catalysts. Concave tetrahedron-like micropores are typical for geomaterials (Fig. 1c). From Fig. 1c it may also be observed that such type of micropores can be formed by dense packing of ellipsoidal particles. For tetrahedron-like inhomogeneities, calculation of effective properties by homogenization schemes based on ellipsoidal shapes still present a challenge, especially for the inverse problem (Popov et al., 2018; Trofimov et al., 2018a). Also it should be noted that to the authors' best knowledge tetrahedron-like shapes have never been considered previously for extensive calculation of their elastic contribution to the overall properties of the medium.

In this paper, we focus mainly on the study of the contribution of tetrahedron-like inhomogeneities to the overall elastic properties of composites. The considered inhomogeneities are shaped like regular tetrahedrons, but with spherical polygons as faces. The governing parameter of the shape is the sphericity parameter $p = R_0/R_S$ (Traxl and Lackner, 2018), where R_0 is the distance between the center of the tetrahedron and its vertices; R_S is the radius of the sphere on which the spherical polygons are formed. It covers both convex ($p \geq 0$) and concave shapes ($p < 0$), see Fig. 2 for examples. The axis x_3 coincides with one of the axes of the tetrahedron, while the axis x_1 coincides with the projection of another axis of the tetrahedron.

Traditionally, estimation of effective elastic properties is based on the Eshelby theory (Eshelby, 1961, 1957) where the inhomogeneity is considered as ellipsoidal for which analytical solution is available. Meanwhile, non-ellipsoidal inhomogeneities are widely presented in many man-made and natural materials for which only a limited number of analytical solutions are available due to the complexity of boundary value problem. Most of these results have been obtained for 2-D shapes using complex variable approach (see, for example Kachanov et al., 1994) . In 3-D, some results have been obtained for cracks of irregular shapes (see the review in Kachanov and Sevostianov, 2018), The toroidal shape was studied by Argatov and Sevostianov (2011), who approximated the contribution of a thin rigid toroidal inhomogeneity to the overall stiffness. Their result was generalized to the case of a torus of arbitrary shape by Krasnitskii et al. (2018). The problem of the effective conductivity (thermal or electric) of a material containing toroidal insulating inhomogeneities was addressed by Radi and Sevostianov (2016).

* Corresponding author.
E-mail address: a.markov@skoltech.ru (A. Markov).

https://doi.org/10.1016/j.ijsolstr.2019.02.020
0020-7683/

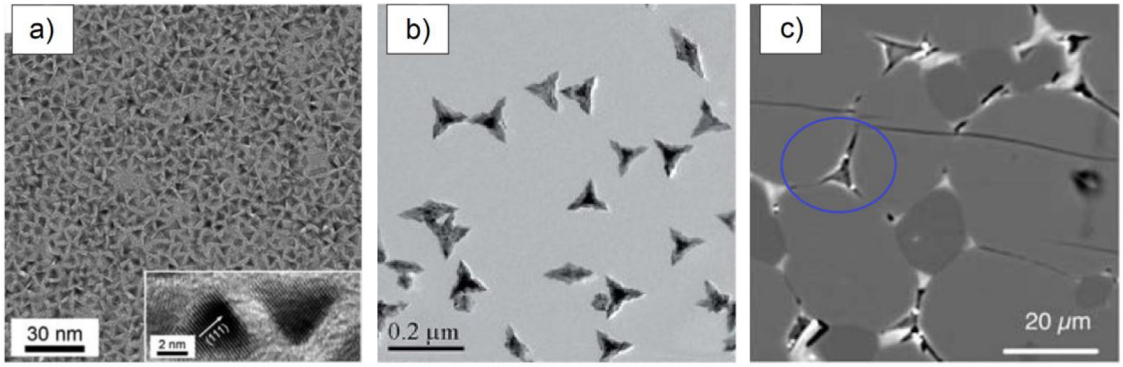

Fig. 1. Examples of tetrahedron-like inhomogeneities: (a) tetrahedral Rh nanoparticles (Park et al., 2007), (b) concave tetrahedral Pd nanocrystals (Li et al., 2017), (c) pores in harzburgite (Wark et al., 2003).

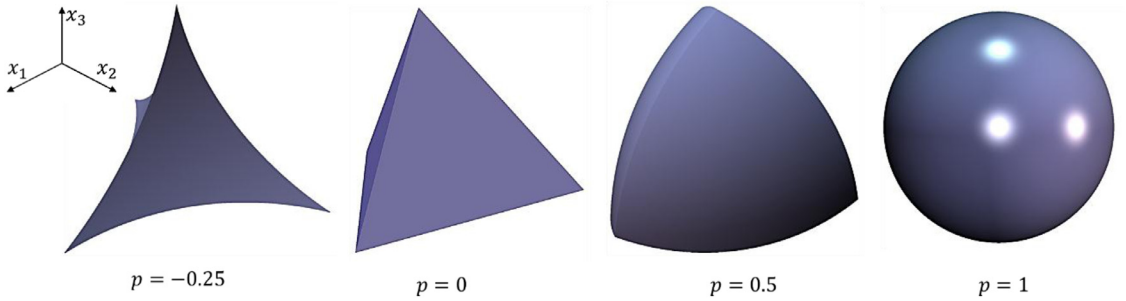

Fig. 2. Example of tetrahedron-like shapes.

Pure numerical and supplemented with analytical approximations results for non-ellipsoidal inhomogeneities are also used to obtain contribution to the effective properties from the single inhomogeneity. In the case of concave shapes described analytically, Sevostianov et al. (2008) calculated contribution from the superspherical pores using the Finite Element Method (FEM). Based on this data, analytical approximations were built in Sevostianov and Giraud (2012) and further used to calculate overall elastic properties of oolitic rock (Sevostianov and Giraud, 2013). This approach, however is based on computational results taken from Sevostianov et al. (2008) where the accuracy and stability of the calculations are rather poor. Recently, in Chen et al. (2015), authors numerically calculated compliance tensors of superspherical pores and provided analytical approximations of these tensors using solution for spherical pore. Since sphere is isotropic, approximations based on it were not able to account for cubic symmetry of the most superspherical shapes (except sphere) and, thus, more accurate approximation was proposed in Trofimov et al. (2018a). Another analytical concave shape – supersphere of revolution – was considered by Sevostianov et al. (2016). For the case of 3D irregular pore shapes in carbon-carbon composites, Drach et al. (2011) used the FEM to calculate the compliance contribution tensors. Garboczi and Douglas (2012) developed numerical approximations for intrinsic bulk and shear moduli in the case of randomly oriented block-like particles based on finite element calculations and corrected analytical solution for an ellipsoid. The effects of spherical, cubic, tetrahedral and octahedral particle shapes on the effective thermoelastic properties of materials with matrix-inclusion topology were discussed in Rasool and Böhm (2012). Statistical model correlating compliance contribution tensors of pore shapes with their geometrical parameters was proposed in Drach et al. (2014). Trofimov et al. (2017b) used finite element calculations to analyze the effect of shape of several representative convex polyhedra on the overall elastic properties of particle-reinforced composites. The problem of helical fiber in the context of its waviness and elastic contrast effect was studied using the FEM (Trofimov et al., 2017a; Trofimov and Sevostianov, 2017).

An alternative numerical technique to the FEM is the mesh-free Volume Integral Equation Method (VIEM). The problem is formulated in terms of volume integral equations for strain and stress fields in an elastic medium. These equations are discretized on a regular grid of approximating nodes by the Gaussian functions centered at the nodes. The theory of approximation by Gaussian and other similar functions was developed by Maz'ya and Schmidt (2007). This method was first developed by Kanaun (2009) for homogenization of 2D-materials with inhomogeneities of arbitrary shapes; it was adapted for 3D-materials in Kanaun (2011). Kanaun and Pervago (2011) used this technique for composites with periodic and random sets of spherical inhomogeneities with a step-wise change of the elastic properties. Markov and Kanaun (2017, 2018) applied the VIEM to the study of interaction of isolated and intersecting planar cracks and spherical inhomogeneities.

In our work, we numerically calculate compliance contribution tensors for geometrically comprehensive set of tetrahedron-like inhomogeneities covering both convex and concave shapes, for various combinations of matrix/inhomogeneity properties including softer and stiffer cases. Results obtained by two numerical techniques: the FEM or the VIEM are compared (similarly to a recent paper of Trofimov et al., 2018b).

In our work, we also consider the problem of predicting the change in contribution to the overall elastic properties from inhomogeneities with identical shapes but different material properties, the so-called replacement relations. Application of the replacement relations for geophysics was first addressed by Gassman (1951), who proposed to express the bulk modulus K of fully saturated rock in terms of the elastic properties of dry rock (see Mavko et al., 2009; Jaeger et al., 2007).This approach was further developed in the works of Ciz and Shapiro (2007), au-

thors obtained similar results for shear modulus, and Saxena and Mavko (2014), who derived replacement relations (they used term "substitution relations") for isotropic rocks containing inhomogeneities of the same shape, but different elastic constants. In the context of property contribution tensors, this problem was addressed by Sevostianov and Kachanov (2007), who derived explicit relations that are exact for ellipsoids. Recently replacement relations for thermal conductivities of composite materials having different matrices were proposed and verified numerically by Sevostianov et al. (2018). Application of the replacement relations to polyhedral inclusions of different shapes was realized by Trofimov et al. (2017b). In this work, the worst results of application of replacement relation were obtained for tetrahedral shape; however, "smoothing" of the edges improved considerably the results.

In this paper, the accuracy of replacement relations approximations for various shape and material combinations is analyzed and possible analytical functions improving their accuracy are presented.

2. Elastic properties contribution tensors

For materials containing inhomogeneities, it is possible to express the effective elastic properties in terms of the so-called property contribution tensors of an individual inhomogeneity. Such tensors were first introduced in the context of contributions of pores and cracks to elastic properties by Horii and Nemat-Nasser (1983). Later, the concept has been extended to inhomogeneities of various shapes and generalized for the other physical properties (conductivity, thermal expansion, diffusion) in the works of Sevostianov and Kachanov (2002,2001).

Let us consider an infinite homogeneous elastic medium containing both matrix material and regularly distributed identical isolated inhomogeneities that occupy a volume fraction ϕ. Following the work of Kachanov et al. (1994), the volume-averaged strain in such medium subjected to a constant external stress field $\boldsymbol{\sigma}^0$ in terms of the extra strain $\Delta\boldsymbol{\varepsilon}$ due to the presence of inhomogeneities takes the form

$$\langle\varepsilon\rangle = \mathbf{S}^0 : \sigma^0 + \Delta\varepsilon. \tag{2.1}$$

Here $\mathbf{S}^0$ is the compliance tensor of the matrix and $\Delta\boldsymbol{\varepsilon}$ is the extra strain due to the presence of inhomogeneity; $\Delta\boldsymbol{\varepsilon}$ can be expressed as a function of the remotely applied stress $\boldsymbol{\sigma}^0$:

$$\Delta\varepsilon = \varphi\mathbf{H} : \sigma^0, \tag{2.2}$$

where $\mathbf{H}$ is the fourth-rank compliance contribution tensor of the inhomogeneities normalized by their volume fraction. The tensor $\mathbf{H}$ can be expressed through the following integral (Kanaun and Levin, 2008)

$$\mathbf{H} = -\mathbf{S}^0 \frac{1}{V^1} \int_{V^1} \mathbf{C}^{10}(x) : \mathbf{A}(x)dx, \tag{2.3}$$

where $\mathbf{C}^{10}(x) = \mathbf{C}^1 - \mathbf{C}^0$, $x \in V^1$; $\mathbf{C}^{10}(x) = 0$, $x \notin V^1$, $\mathbf{C}^0$ and $\mathbf{C}^1$ are the stiffness tensors of the matrix and the inclusions correspondingly, V^1 is the volume occupied by a single inclusion. The fourth rank tensor $\mathbf{A}(x)$ is defined as

$$\varepsilon(x) = \mathbf{A}(x) : \sigma^0, \tag{2.4}$$

where $\boldsymbol{\varepsilon}(x)$ is the strain field inside the inclusion. It should be noted that the tensor $\mathbf{A}(x)$ depends not only on the elastic properties, but also on the shape of the inclusion.

In order to calculate the compliance contribution tensor $\mathbf{H}$ of a single inhomogeneity, one has to consider the limit $\varphi \to 0$, i.e., an infinite homogeneous host medium with an isolated inhomogeneity subjected to a constant external stress.

Similarly, Eq. (2.1) can be rewritten for the case of applied strain field $\boldsymbol{\varepsilon}^0$ (Sevostianov and Kachanov, 1999). In this case, the volume-averaged stress can be represented as follows:

$$\langle\sigma\rangle = \mathbf{C}^0 : \varepsilon^0 + \Delta\sigma. \tag{2.5}$$

Here $\Delta\boldsymbol{\sigma}$ is the extra stress due to the presence of the inhomogeneity:

$$\Delta\sigma = \varphi\mathbf{N} : \varepsilon^0, \tag{2.6}$$

where $\mathbf{N}$ is the fourth-rank stiffness contribution tensor of the inhomogeneities normalized by their volume fraction. The tensor $\mathbf{N}$ can be defined in a similar way to the tensor $\mathbf{H}$ (see Eq. (2.3)).

It should be noted that the stiffness and compliance contribution tensors $\mathbf{N}$ and $\mathbf{H}$ are interrelated as:

$$\mathrm{N} = -\mathrm{C}^0 : \mathbf{H} : \mathrm{C}^0. \tag{2.7}$$

Thus, to evaluate the contribution of an inhomogeneity to the overall response of a material, one needs to solve the problem of an infinite elastic medium containing considered inhomogeneity subjected to constant external stress $\boldsymbol{\sigma}^0$ or strain $\boldsymbol{\varepsilon}^0$ field.

The effective compliance tensor $\mathbf{S}^*$ of a composite material containing multiple inhomogeneities can be expressed as

$$\mathbf{S}^* = \mathbf{S}^0 + \Delta\mathbf{S}^{RVE}, \tag{2.8}$$

where $\Delta\mathbf{S}^{RVE}$ is the total compliance contribution of all the inhomogeneities present in a Representative Volume Element (RVE).

In the case of dilute concentrations of inhomogeneities, the non-interaction scheme is applicable; and $\Delta\mathbf{S}^{RVE}$ is found by direct summation of contributions from all individual inhomogeneities in the RVE that occupies the volume V:

$$\Delta\mathbf{S}^{RVE} = \frac{1}{V}\sum_i V^{(i)}\mathbf{H}^{(i)}, \tag{2.9}$$

where $V^{(i)}$ and $\mathbf{H}^{(i)}$ are the volume and the compliance contribution tensor of the ith inhomogeneity, respectively.

When interaction between inhomogeneities cannot be neglected, more advanced techniques should be used, for instance, the Mori-Tanaka scheme (Benveniste, 1987; Mori and Tanaka, 1973). In the framework of this scheme, contribution of all inhomogeneities to the overall compliance of the RVE is given by

$$\Delta\mathbf{S}^{RVE} = \left[\frac{1}{V}\sum_i V^{(i)}\mathbf{H}^{(i)}\right] : \left[\frac{1}{V}\sum_i V^{(i)}\left(\mathbf{S}^{(i)} - \mathbf{S}^0\right)^{-1} : \mathbf{H}^{(i)} + \varphi\mathbf{J}\right]^{-1}, \tag{2.10}$$

where $\mathbf{S}^{(i)}$ is the compliance tensor of the material of the ith inhomogeneity and $\mathbf{J}$ is the fourth order unit tensor.

3. Numerical calculation of H-tensor

Due to irregularity of the considered inhomogeneity shapes that are described in Section 1, only numerical methods are applicable for the calculation of the $\mathbf{H}$-tensor. In this Section, we discuss numerical solutions obtained by using FEM and VIEM approaches for individual tetrahedral-like inhomogeneities.

3.1. FEM calculation of H-tensor components of the considered shapes

In the Finite Element Method (FEM) procedure, we calculate compliance contribution tensor ($\mathbf{H}$) simulating the given particle geometry in a large volume V subjected to uniform displacement boundary conditions on ∂V: $\mathbf{u}|_{\partial V} = \boldsymbol{\varepsilon}^0 \cdot \mathbf{x}$. To perform the necessary steps, we prepare 3D FEM mesh for the analysis by generating the surface mesh of the particle with approximately hundred thousands of elements in a custom MATLAB script (Trofimov et al., 2017a).

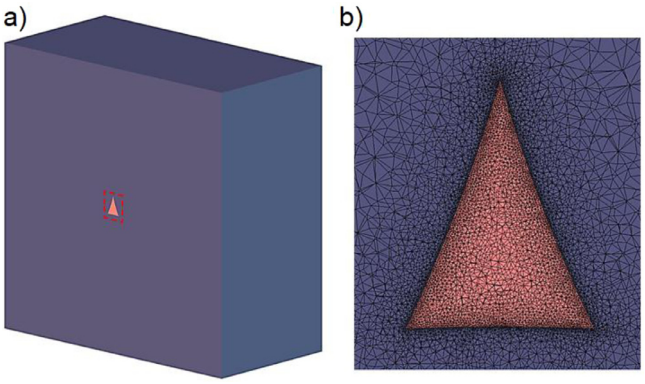

Fig. 3. Example of a mesh density of the matrix and tetrahedral-like inhomogeneity with $p = 0.25$: (a) general view; (b) close-up view of the highlighted region.

The setup with a single shape inside the cubical reference volume (cube sides are 10 times larger than the diameter of the particle) is then auto meshed with non-linear tetrahedral 3D elements (tetra10) due to higher accuracy of results compared to linear elements (tetra4), see Fig. 3 for mesh density example. Note, that the choice of the reference volume size used in the analysis is based on a sensitivity study performed for a particle of spherical shape, for which an analytical solution is available in the literature.

After the volume mesh is generated, the non-zero components of compliance contribution tensor (**H**) are calculated from the post-processing the results of the set of six load cases: three normal loadings (in the directions of three global coordinate axes) and three shear loadings. The procedure is realized using a custom Python script, as described in Drach et al. (2011). The script starts with calculating the average stress components within the volume for each load case:

$$\langle \sigma_{ij} \rangle_m = \frac{1}{V} \sum_{l=1}^{N} \left(\sigma_{ij}^{(l)} \right)_m \cdot V^{(l)}, (i, j = 1, 2, 3; k = 1, 2, ..., 6) \tag{3.1}$$

where $\langle \sigma_{ij} \rangle_m$ is the volume average of the stress component ij calculated from the results of the mth load case, $(\sigma_{ij}^{(l)})_m$ is the stress component ij at the centroid of the finite element l calculated from the mth load case, $V^{(l)}$ is the volume of the element l, and N is the total number of elements in the model. At the next step we obtain components of compliance contribution tensor as follows:

$$H_{mnpq} = -S_{mnij}^{(0)} \left[\frac{(\sigma_{ij}^0)_m - \langle \sigma_{ij} \rangle_m}{(\varepsilon_{kl}^0)_m} \right] S_{klpq}^{(0)}, \tag{3.2}$$

where $S_{mnij}^{(0)}$ are the components of the given matrix compliance tensor, $(\varepsilon_{kl}^0)_m$ and $(\sigma_{ij}^0)_m$ are prescribed components of strain and stress, respectively.

3.2. Mesh-free calculation of H-tensor components of the considered shapes

In order to calculate the compliance contribution tensor **H**, we consider the mesh-free VIEM. We formulate the problem in terms of integral equations for strain and stress (see, e.g., Kanaun and Levin, 2008):

$$\varepsilon_{ij}(x) + \int K_{ijkl}(x - x') C_{klmn}^{10}(x') \varepsilon_{mn}(x') dx' = \varepsilon_{ij}^0(x), \tag{3.3}$$

$$\sigma_{ij}(x) - \int S_{ijkl}(x - x') S_{klmn}^{10}(x') \sigma_{mn}(x') dx' = \sigma_{ij}^0(x), \tag{3.4}$$

where $\mathbf{S}^{10}(x) = \mathbf{S}^1 - \mathbf{S}^0$, $x \in V^1$; $\mathbf{S}^{10}(x) = 0$, $x \notin V^1$, $\mathbf{S}^0$ and $\mathbf{S}^1$ are the compliance tensors of the matrix and the inclusions correspondingly. The kernels $\mathbf{K}(x)$ and $\mathbf{S}(x)$ are calculated from the second derivative of Green's function $\mathbf{G}(x)$ of the matrix:

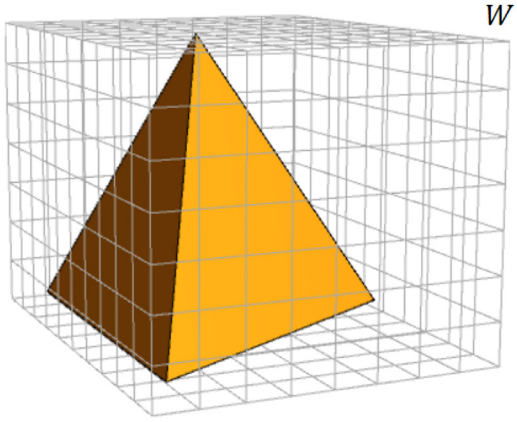

Fig. 4. A volume of a medium containing a tetrahedral inclusion covered by a regular grid of nodes.

$$K_{ijkl}(x) = -\left[\partial_i \partial_k G_{jl}(x) \right]_{(ij)(kl)}, \tag{3.5}$$

$$S_{ijkl}(x) = C_{ijkl}^0 K_{mnpq}(x) C_{pqkl}^0 - C_{ijkl}^0 \delta(x). \tag{3.6}$$

Here $\delta(x)$ is Dirac's delta function. The properties of these kernels were studied by Kanaun (1981) and Kunin (1983).

For discretization of the integral Eqs. (3.3) and (3.4), a class of Gaussian approximation functions is used. Approximate solutions of Eqs. (3.3) and (3.4) are presented in the following forms:

$$\varepsilon_{ij}(x) \approx \sum_{s=1}^{N} \varepsilon_{ij}^{(s)} \varphi\left(x - x^{(s)}\right), \tag{3.7}$$

$$\sigma_{ij}(x) \approx \sum_{s=1}^{N} \sigma_{ij}^{(s)} \varphi\left(x - x^{(s)}\right), \tag{3.8}$$

where $\boldsymbol{\varepsilon}^{(s)}$ and $\boldsymbol{\sigma}^{(s)}$ are unknown values of strain and stress at the node $x^{(s)}$ ($s = 1, 2, ..., N$) of a regular grid that covers a cuboid W, (Fig. 4) that contains the region V_1 occupied by the inclusion, N is the total number of the nodes in W.

The function $\varphi(x)$ is a 3D-Gaussian distribution function:

$$\varphi(x) = \frac{1}{(\pi H)^{3/2}} \exp\left(-\frac{|x|^2}{Hh^2} \right), \tag{3.9}$$

where h is the grid step, H is a non-dimensional parameter of the order of 1; for the considered calculations $H = 2$.

After substituting the solutions (3.7) and (3.8) into the integral Eqs. (3.3) and (3.4), respectively, we obtain the following systems of linear equations:

$$\varepsilon_{ij}^{(r)} + \sum_{s=1}^{N} \Pi_{ijkl}^{(r,s)} C_{klmn}^{10(s)} \varepsilon_{mn}^{(s)} = \varepsilon_{ij}^{0(r)}, \quad r = 1, \ldots, N \tag{3.10}$$

$$\Pi_{ijkl}^{(r,s)} = \Pi_{ijkl}\left(x^{(r)} - x^{(s)}\right), \; C_{ijkl}^{10(s)} = C_{ijkl}^{10}\left(x^{(s)}\right), \; \varepsilon_{ij}^{0(s)} = \varepsilon_{ij}^0\left(x^{(s)}\right), \tag{3.11}$$

$$\sigma_{ij}^{(r)} - \sum_{s=1}^{N} \Gamma_{ijkl}^{(r,s)} S_{klmn}^{10(s)} \sigma_{mn}^{(s)} = \sigma_{ij}^{0(r)}, \tag{3.12}$$

$$\Gamma_{ijkl}^{(r,s)} = \Gamma_{ijkl}\left(x^{(r)} - x^{(s)}\right), \; S_{ijkl}^{10(s)} = S_{ijkl}^{10}\left(x^{(s)}\right), \; \sigma_{ij}^{0(s)} = \sigma_{ij}^0\left(x^{(s)}\right), \tag{3.13}$$

The integral operators $\mathbf{\Pi}(x)$ and $\mathbf{\Gamma}(x)$ are:

$$\Pi_{ijkl}(x) = \int K_{ijkl}(x - x')\varphi(x')dx', \tag{3.14}$$

$$\Gamma_{ijkl}(x) = \int S_{ijkl}(x - x')\varphi(x')dx'. \tag{3.15}$$

The integrals in (3.14) and (3.15) can be calculated explicitly if evaluated over the entire 3D-space; this is possible due to the fact that Gaussian distribution functions decrease very fast (see, e.g., Kanaun and Pervago, 2011). Also, the left-hand side matrices of the systems of linear Eqs. (3.10) and (3.12) have Toeplitz's structure; as a result, only one row and one column must be stored in computer memory. For the numerical solution of these systems, only Krylov subspace iterative methods (Conjugate Gradient, Minimal Residue or their derivatives) are viable (Kanaun et al., 2013). These methods require calculation of matrix-vector products at every iteration; for this calculation the fast Fourier transform technique may be used (Golub and van Loan, 1996; Kanaun, 2009).

It should also be noted that in the case the Young's modulus of the inclusion E^1 is lower than the Young's modulus of the matrix E^0, the system (3.10) converges faster than the system (3.12), while in the case E^1 is higher than E^0, the system (3.12) is more efficient (Kanaun and Pervago, 2011). This may be explained by the fact that relatively low values of E^1 result in a low stress (tending to zero at $E^1 \to 0$), while high values of E^1 result in a low strain (tending to zero at $E^1 \to \infty$).

Once either of two systems, (3.10) or (3.12), is solved, the compliance contribution tensor $\mathbf{H}$ may be calculated by the procedure described in previous Sections.

3.3. Numerical results

In this section we consider tetrahedron-like inhomogeneities (Fig. 2). The results are given in terms of the sphericity parameter p; the corresponding approximate values of the volume V^1 of the unit inhomogeneity (i.e., the distance R from the center of the inclusion to any of its vertices is unitary) are given in Table 1.

Comparison of calculations of the compliance contribution tensor $\mathbf{H}$ by the FEM analysis and by the VIEM is given in Table 2 for absolutely rigid inclusions and in Table 3 for pores. For the VIEM, a uniform node grid with the step $h/R = 0.01$ was used; such node grid corresponds approximately to 6 million nodes. For simplicity, the system of linear Eqs. (3.12) was used for the solution, as testing has shown that both systems (3.10) and (3.12) give similar result.

It may be noted that both numerical techniques have given very close results; in most cases the difference is less than 2%. Also, the results of both techniques practically coincide with the exact results for the case of sphere ($H_{1111} = H_{3333} = -2.031, H_{1133} = H_{1122} = 0.693$, $H_{1313} = -1.362$ for the rigid sphere and $H_{1111} = H_{3333} = 2.0, H_{1133} = H_{1122} = -0.477$, $H_{1313} = 1.239$ for the spherical pore). Only in the extreme case of a rigid inclusion of very concave shape ($p \leq -0.2$) the difference is about 10%. Comparison of the results obtained by the two considered numerical methods for the contrast E^1/E^0 that is equal to 10, 5, 2, 0.5, 0.2, and 0.1 is given in Appendix A.

4. Replacement relations

In this Section, we check the applicability of the replacement relations to the numerical solutions obtained in the previous Section. To improve the quality of calculations, we introduce the so-called adjustment tensor.

4.1. Replacement relations formulation

The general case of replacement relations (Sevostianov and Kachanov, 2007) allows one to interrelate the effective compliance and stiffness tensors of inhomogeneities "A" and "B" of the same ellipsoidal shape (and embedded into the same matrix) but with different elastic constants

$$\frac{V_1}{V}\left(\mathrm{H}_A^{-1} - \mathrm{H}_B^{-1}\right) = \left(\mathrm{S}^A - \mathrm{S}^0\right)^{-1} - \left(\mathrm{S}^B - \mathrm{S}^0\right)^{-1}, \tag{4.1}$$

$$\frac{V_1}{V}\left(\mathrm{N}_A^{-1} - \mathrm{N}_B^{-1}\right) = \left(\mathrm{C}^A - \mathrm{C}^0\right)^{-1} - \left(\mathrm{C}^B - \mathrm{C}^0\right)^{-1}. \tag{4.2}$$

Here N_A and N_B are the stiffness contribution tensors and H_A and H_B are the compliance contribution tensors of inhomogeneities with material properties "A" and "B", respectively. Similarly, C^A and C^B are the stiffness tensors, S^A and S^B are the compliance tensors of these inhomogeneities.

In two particular cases, if the material "B" is either absolutely rigid or represents a pore, the comparison relations take the form:

$$\frac{V_1}{V}\left(\mathrm{H}_A^{-1} - \mathrm{H}_{pore}^{-1}\right) = \left(\mathrm{S}^A - \mathrm{S}^0\right)^{-1}, \tag{4.3}$$

$$\frac{V_1}{V}\left(\mathrm{N}_A^{-1} - \mathrm{N}_{rigid}^{-1}\right) = \left(\mathrm{C}^A - \mathrm{C}^0\right)^{-1}. \tag{4.4}$$

Table 1
Approximate volume V^1 of the unit tetrahedron-like inhomogeneity for different values of the parameter p.

p	−0.3	−0.25	−0.2	−0.15	−0.1	0	0.25	0.5	0.75	1
V^1	0.135	0.184	0.24	0.301	0.367	0.511	0.948	1.512	2.332	4.189

Table 2
Independent components of the compliance contribution tensor H_{ijkl} of rigid inhomogeneities.

	$E^1/E^0 \to \infty$									
p	H_{1111}^{FEM}	H_{1111}^{VIEM}	H_{3333}^{FEM}	$H_{3333}^{VIEM} H_{3333}^{GA}$	H_{1122}^{FEM}	$H_{1122}^{VIEM} H_{1122}^{GA}$	H_{1133}^{FEM}	$H_{1133}^{VIEM} H_{1133}^{GA}$	H_{1313}^{FEM}	$H_{1313}^{VIEM} H_{1313}^{GA}$
−0.3	−5.505	−4.868	−5.685	−4.987	2.188	1.930	2.370	2.053	−3.846	−3.386
−0.25	−4.834	−4.365	−4.972	−4.505	1.898	1.716	2.032	1.783	−3.366	−3.049
−0.2	−4.333	−3.986	−4.436	−4.066	1.682	1.539	1.780	1.602	−3.007	−2.761
−0.15	−3.956	−3.837	−4.033	−3.923	1.520	1.477	1.591	1.531	−2.738	−2.671
−0.1	−3.661	−3.652	−3.719	−3.698	1.393	1.389	1.445	1.438	−2.527	−2.507
0	−2.954	−2.929	−3.005	−2.984	1.060	1.051	1.096	1.093	−2.022	−1.988
0.25	−2.642	−2.616	−2.645	−2.634	0.955	0.941	0.957	0.949	−1.792	−1.798
0.5	−2.321	−2.353	−2.325	−2.365	0.814	0.830	0.821	0.836	−1.554	−1.604
0.75	−2.129	−2.154	−2.132	−2.160	0.732	0.745	0.738	0.749	−1.420	−1.452
1	−2.030	−2.030	−2.030	−2.030	0.693	0.692	0.693	0.692	−1.362	−1.361

Table 3
The same as in Table 2 for pores.

	$E^1/E^0 = 0$									
p	H_{1111}^{FEM}	H_{1111}^{VIEM}	H_{3333}^{FEM}	H_{3333}^{VIEM}	H_{1122}^{FEM}	H_{1122}^{VIEM}	H_{1133}^{FEM}	H_{1133}^{VIEM}	H_{1313}^{FEM}	H_{1313}^{VIEM}
−0.3	2.827	2.913	2.699	2.786	−0.553	−0.570	−0.423	−0.480	1.820	1.882
−0.25	2.802	2.863	2.679	2.743	−0.550	−0.562	−0.423	−0.470	1.804	1.847
−0.2	2.767	2.808	2.650	2.686	−0.545	−0.555	−0.424	−0.469	1.780	1.807
−0.15	2.723	2.750	2.614	2.663	−0.540	−0.549	−0.425	−0.466	1.750	1.771
−0.1	2.676	2.692	2.574	2.622	−0.535	−0.541	−0.426	−0.465	1.717	1.735
0	2.597	2.621	2.544	2.601	−0.525	−0.526	−0.430	−0.463	1.670	1.715
0.25	2.339	2.371	2.287	2.346	−0.504	−0.510	−0.444	−0.464	1.485	1.524
0.5	2.164	2.184	2.137	2.168	−0.491	−0.500	−0.458	−0.467	1.363	1.385
0.75	2.049	2.064	2.041	2.054	−0.482	−0.486	−0.469	−0.472	1.282	1.293
1	2.002	2.002	2.002	2.002	−0.476	−0.476	−0.476	−0.476	1.239	1.239

Table 4
Comparison of the component H_{1111} of the compliance contribution tensor calculated by the replacement relation from an inhomogeneity "B" that is absolutely rigid with the same component calculated by the VIEM method.

	E^A/E^0							
p	∞ (rigid)	10	5	2	0.5	0.2	0.1	0 (void)
	H_{1111}^{RRigid}							
−0.3	−4.868	−3.129	−2.166	−0.821	0.565	0.984	1.142	1.310
−0.25	−4.365	−2.918	−2.065	−0.807	0.571	1.003	1.167	1.342
−0.2	−3.986	−2.747	−1.979	−0.793	0.578	1.023	1.195	1.380
−0.15	−3.837	−2.677	−1.942	−0.788	0.581	1.033	1.209	1.398
−0.1	−3.652	−2.587	−1.896	−0.780	0.585	1.046	1.226	1.421
0	−2.929	−2.208	−1.686	−0.743	0.606	1.116	1.322	1.550
0.25	−2.616	−2.025	−1.578	−0.721	0.622	1.169	1.398	1.656
0.5	−2.353	−1.865	−1.479	−0.700	0.638	1.228	1.483	1.777
0.75	−2.154	−1.739	−1.399	−0.682	0.654	1.286	1.569	1.902
1	−2.030	−1.658	−1.347	−0.669	0.665	1.330	1.633	2.002
	ΔH_{1111}^{VIEM}, %							
−0.3	0.0	42.406	35.807	18.620	−18.161	−35.165	−43.504	−55.047
−0.25	0.0	34.509	30.182	16.613	−16.887	−33.258	−41.744	−53.106
−0.2	0.0	27.240	25.497	14.841	−15.577	−31.156	−39.190	−50.848
−0.15	0.0	24.242	23.482	14.295	−14.910	−30.360	−37.838	−49.176
−0.1	0.0	22.552	20.910	13.607	−14.204	−29.342	−36.395	−47.226
0	0.0	11.442	12.639	8.404	−10.889	−24.272	−31.044	−40.838
0.25	0.0	7.987	8.846	5.969	−7.849	−17.853	−22.793	−30.736
0.5	0.0	4.778	5.341	3.680	−4.806	−11.217	−14.146	−19.059
0.75	0.0	2.246	2.496	1.731	−2.010	−4.959	−5.920	−7.868
1	0.0	0.029	0.067	0.022	−0.088	−0.134	−0.262	0.003

It should be noted that relations (4.1) and (4.2) are exact only for inhomogeneities of ellipsoidal shape; however, it was shown by Chen et al. (2017) that these relations give a good approximation for non-ellipsoidal convex superspheres as well.

4.2. Numerical results

In the current work, we apply the replacement relations to tetrahedral-like shapes described in Section 1. First, we consider absolutely rigid material as the material "B"; we take the compliance contribution tensor **H** obtained by the VIEM for each inhomogeneity shape from the Section 3.3. Then we apply the replacement relation for the calculation of the tensor **H** of the inhomogeneity "A" of the same shape, for different values of contrast E^A/E^0 of Young's moduli of the matrix and material "A". Comparison of the results obtained for the component H_{1111} of the compliance contribution tensor by using the replacement relation and the VIEM numerical solution is given in the Table 4; for the comparison, we use the $\Delta H_{ijkl}^{VIEM} = (H_{ijkl}^{RRigid,RPore} - H_{ijkl}^{VIEM})/H_{ijkl}^{VIEM}$ ratios. Here H_{ijkl}^{RRigid} and H_{ijkl}^{RPore} are the compliance contribution tensors calculated by the replacement relation from an inhomogeneity "B" that is absolutely rigid or represents a pore, correspondingly. The results for the other independent components of the tensor **H** appear in Appendix B; these results follow the same trend as the component H_{1111}.

It may be clearly seen that the replacement relation gives acceptable results for the material "A" stiffer than the matrix in the case of convex shapes ($p > 0$), however, for concave shapes the results differ by a large margin ($> 20\%$ in most cases). It is also important to note that in the case of the material "A" softer than the matrix results obtained by the replacement relation do not follow the correct trend of the corresponding numerical results; i.e., the corresponding component H_{1111} decreases for smaller values of parameter p, while it should increase.

Similar comparison of the results obtained for the component H_{1111} by using the replacement relation and the numerical solution in the case where the material "B" represents a pore is given in the Table 5.

Here one may observe that the replacement relation has given us much better results for the material "A" softer than the matrix, the difference between the values is lower than 10% even in the case of very concave shapes. From the other hand, if the material "A" is stiffer than the matrix, the results given by the replacement relation do not follow the correct trend (the results decrease for smaller p).

Table 5
The same as in Table 4 for calculation by the replacement relation from an inhomogeneity "B" that represents a pore.

	E^A/E^0							
p	∞ (rigid)	10	5	2	0.5	0.2	0.1	0 (void)
	H_{1111}^{RPore}							
−0.3	−1.562	−1.332	−1.123	−0.609	0.739	1.669	2.185	2.913
−0.25	−1.578	−1.343	−1.131	−0.611	0.735	1.652	2.156	2.863
−0.2	−1.595	−1.356	−1.140	−0.614	0.732	1.634	2.126	2.808
−0.15	−1.613	−1.369	−1.149	−0.617	0.728	1.615	2.093	2.750
−0.1	−1.634	−1.383	−1.160	−0.620	0.724	1.595	2.060	2.692
0	−1.660	−1.402	−1.173	−0.623	0.719	1.570	2.018	2.621
0.25	−1.716	−1.442	−1.201	−0.631	0.709	1.519	1.933	2.391
0.5	−1.875	−1.552	−1.276	−0.651	0.685	1.412	1.762	2.196
0.75	−1.974	−1.620	−1.321	−0.663	0.672	1.358	1.677	2.064
1	−2.030	−1.658	−1.347	−0.669	0.665	1.330	1.633	2.002
	ΔH_{1111}^{VIEM}, %							
−0.3	−67.908	−39.384	−29.576	−11.995	7.100	9.993	8.115	0.0
−0.25	−63.844	−38.082	−28.675	−11.605	7.047	9.952	7.631	0.0
−0.2	−59.981	−37.208	−27.699	−11.135	6.954	9.903	8.127	0.0
−0.15	−57.950	−36.458	−26.928	−10.510	6.667	8.844	7.647	0.0
−0.1	−55.263	−34.465	−26.031	−9.760	6.224	7.771	6.874	0.0
0	−43.322	−29.202	−21.632	−9.049	5.636	6.581	5.260	0.0
0.25	−34.396	−23.115	−17.179	−7.278	5.011	6.792	6.768	0.0
0.5	−20.303	−12.775	−9.124	−3.547	2.124	2.138	1.999	0.0
0.75	−8.336	−4.722	−3.186	−1.081	0.710	0.368	0.596	0.0
1	−0.002	0.029	0.067	0.022	−0.088	−0.134	−0.262	0.0

Table 6
Comparison of the component H_{1111} of the compliance contribution tensor calculated by the replacement relation combined with the corresponding adjustment tensor with the same component calculated by the VIEM method.

	E^A/E^0							
p	∞ (rigid)	10	5	2	0.5	0.2	0.1	0 (void)
	$H_{1111}^{RRigid*}$				H_{1111}^{RPore*}			
−0.3	−4.868	−2.504	−1.737	−0.661	0.681	1.536	2.009	2.913
−0.25	−4.365	−2.362	−1.675	−0.657	0.679	1.525	1.990	2.863
−0.2	−3.986	−2.249	−1.623	−0.653	0.679	1.514	1.969	2.808
−0.15	−3.837	−2.215	−1.610	−0.655	0.677	1.502	1.945	2.750
−0.1	−3.652	−2.164	−1.588	−0.655	0.676	1.488	1.921	2.692
0	−2.929	−1.888	−1.443	−0.637	0.676	1.475	1.896	2.621
0.25	−2.616	−1.819	−1.418	−0.649	0.678	1.452	1.848	2.391
0.5	−2.353	−1.755	−1.392	−0.659	0.666	1.373	1.713	2.196
0.75	−2.154	−1.711	−1.377	−0.671	0.665	1.343	1.658	2.064
1	−2.030	−1.658	−1.347	−0.669	0.665	1.330	1.633	2.002
	ΔH_{1111}^{VIEM}, %							
−0.3	0.0	13.962	8.918	−4.436	−1.348	1.227	−0.572	0.0
−0.25	0.0	8.888	5.600	−4.997	−1.136	1.540	−0.682	0.0
−0.2	0.0	4.171	2.927	−5.555	−0.799	1.848	0.162	0.0
−0.15	0.0	2.837	2.325	−4.922	−0.745	1.229	0.049	0.0
−0.1	0.0	2.514	1.301	−4.573	−0.809	0.573	−0.296	0.0
0	0.0	−4.688	−3.600	−7.060	−0.658	0.153	−1.129	0.0
0.25	0.0	−3.029	−2.181	−4.709	0.517	2.081	2.062	0.0
0.5	0.0	−1.374	−0.842	−2.366	−0.595	−0.699	−0.806	0.0
0.75	0.0	0.643	0.864	0.134	−0.384	−0.781	−0.564	0.0
1	0.0	0.029	0.067	0.022	−0.088	−0.134	−0.262	0.0

4.3. Adjustment tensors

As it was shown in the previous Section, application of the replacement relation did not give us a good approximation to the numerical results. To improve the quality of the approximation, we propose two adjustment tensors $\boldsymbol{\alpha}^{Rigid}$ and $\boldsymbol{\alpha}^{Pore}$ for every considered shape of the inhomogeneity:

$$\alpha^{Rigid} = \mathbf{H}^{VIEM} : \left(\mathbf{H}^{RRigid}\right)^{-1}, E^A/E^0 > 1, \tag{4.5}$$

$$\alpha^{Pore} = \mathbf{H}^{VIEM} : \left(\mathbf{H}^{RPore}\right)^{-1}, E^A/E^0 < 1. \tag{4.6}$$

Dependence of the components 1111 of the adjustment tensors on the parameter p is given in Figs. 5 and 6 for "stiff" ($E^A/E^0 > 0$) and "soft" ($E^A/E^0 < 0$) inhomogeneities "A", respectively. Other components of the adjustment tensors $\boldsymbol{\alpha}^{Rigid}$ and $\boldsymbol{\alpha}^{Pore}$ have shown similar behavior.

Linear regression analysis performed by InfoStat statistical software has shown that the dependence of all the non-zero components of tensor α on the parameter p may be approximated reasonably well by a linear function (see Figs. 5 and 6). The resulting linear approximations of the non-zero components of the adjustment tensors $\boldsymbol{\alpha}^{Rigid}$ and $\boldsymbol{\alpha}^{Pore}$ for the cases of "stiff" and "soft"

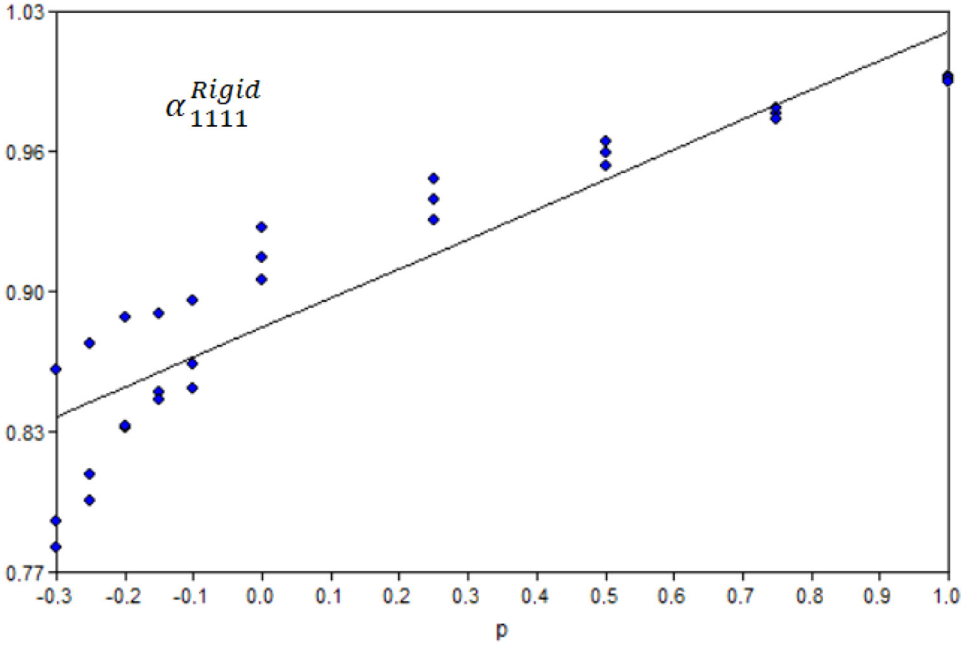

Fig. 5. Dependence of the component α_{1111} of the adjustment tensor on the parameter p in the case of application of the replacement relation from an inhomogeneity "B" that is absolutely rigid and inhomogeneity "A" that is "stiff".

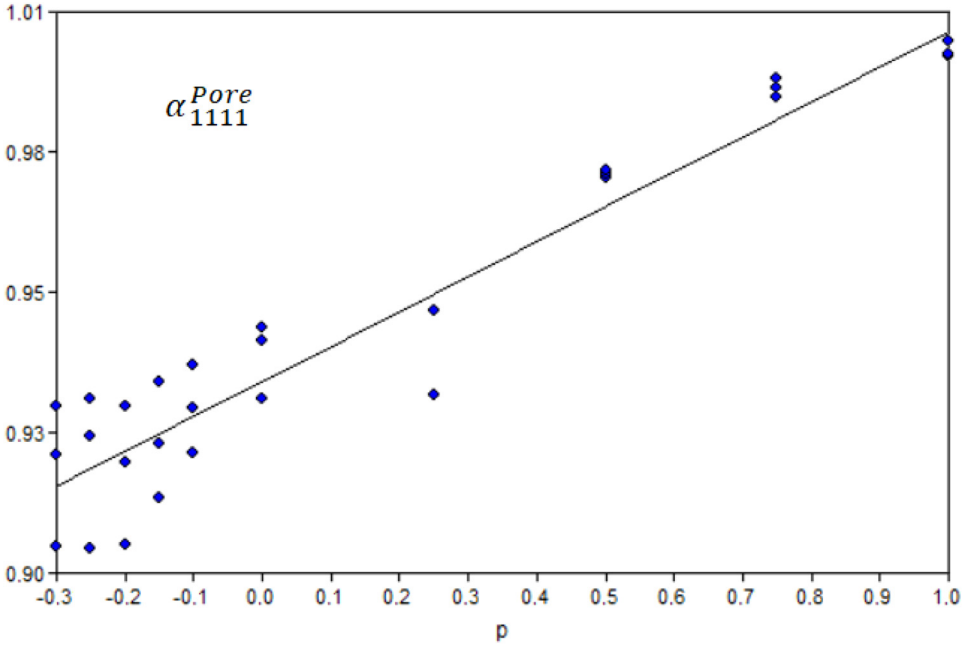

Fig. 6. The same as in Fig. 5 for inhomogeneity "B" that is represents a pore and inhomogeneity "A" that is "soft".

inhomogeneities in Voigt notation are:

$$\begin{aligned}
&\alpha_{11}^{Rigid}(p) = \alpha_{22}^{Rigid}(p) = 0.8808 + 0.1407p,\\
&\alpha_{33}^{Rigid}(p) = 0.8862 + 0.1341p,\\
&\alpha_{12}^{Rigid}(p) = \alpha_{21}^{Rigid}(p) = 0.0415 - 0.0492p,\\
&\alpha_{13}^{Rigid}(p) = \alpha_{23}^{Rigid}(p) = 0.0314 - 0.0391p,\\
&\alpha_{31}^{Rigid}(p) = \alpha_{32}^{Rigid}(p) = 0.0291 - 0.0377p,\\
&\alpha_{44}^{Rigid}(p) = \alpha_{55}^{Rigid}(p) = 0.8388 + 0.1894p,\\
&\alpha_{66}^{Rigid}(p) = 0.8096 + 0.2155p.
\end{aligned} \tag{4.7}$$

$$\begin{aligned}
&\alpha_{11}^{Pore}(p) = \alpha_{22}^{Pore}(p) = 0.9352 + 0.0697p,\\
&\alpha_{33}^{Pore}(p) = 0.9353 + 0.0682p,\\
&\alpha_{12}^{Pore}(p) = \alpha_{21}^{Pore}(p) = -0.0112 + 0.0114p,\\
&\alpha_{13}^{Pore}(p) = \alpha_{23}^{Pore}(p) = -0.0073 + 0.0064p,\\
&\alpha_{31}^{Pore}(p) = \alpha_{32}^{Pore}(p) = -0.0062 + 0.0044p,\\
&\alpha_{44}^{Pore}(p) = \alpha_{55}^{Pore}(p) = 0.9465 + 0.0584p,\\
&\alpha_{66}^{Pore}(p) = 0.9471 + 0.0576p.
\end{aligned} \tag{4.8}$$

We have applied the obtained linear approximations of the adjustment tensors $\boldsymbol{\alpha}^{Rigid}$ and $\boldsymbol{\alpha}^{Pore}$ to improve the results of application of the replacement relations as

$$\mathbf{H}^{RRigid*} = \alpha^{Rigid} : \mathbf{H}^{RRigid}, E^A/E^0 > 1, \tag{4.9}$$

$$\mathbf{H}^{RPore*} = \alpha^{Pore} : \mathbf{H}^{RPore}, E^A/E^0 < 1. \tag{4.10}$$

Comparison of the component 1111 of the corrected **H**-tensors $\mathbf{H}^{RRigid*}$ and $\mathbf{H}^{RPore*}$ to the numerical calculations obtained by the VIEM is given in Table 6. The same comparison for the other independent components of the tensors $\mathbf{H}^{RRigid*}$ and $\mathbf{H}^{RPore*}$ is given in Appendix C.

It may be noted that the application of the adjustment tensors $\boldsymbol{\alpha}^{Rigid}$ and $\boldsymbol{\alpha}^{Pore}$ has improved the results of application of the replacement relations; however, even after the application of these tensors, the resulting **H**-tensor $\mathbf{H}^{RRigid*}$ did not give a good approximation.

5. Conclusions

In this work, we have calculated the individual contribution tensors of elastic properties for a set of tetrahedron-like inhomogeneities with spherical polygons as faces; different values of contrast between the inhomogeneity material and the matrix were considered. For the calculation, two numerical techniques were applied: FEM and VIEM. Both techniques have shown good correspondence (less than 2% of difference for most cases); considerable divergence was observed only in some extreme cases of absolutely rigid strongly concave inclusions. The results have shown that the contribution tensors of tetrahedron-like inhomogeneities are transversally isotropic.

The replacement relations were applied for the calculation of the mentioned contribution tensors for inhomogeneities of the same shape but different Young's moduli from the results obtained for absolutely rigid inhomogeneities and pores. Despite the fact that the replacement relations are strictly valid only for the case of ellipsoidal inclusions, we have obtained good correspondence (less than 10% of difference) in the case of "soft" inclusions, which contributions tensors were calculated from the contribution tensors of pores of the same shape. In the case of "hard" inclusions, whose contributions tensors were calculated from the contribution tensors of absolutely rigid ones, the correspondence was much worse. In the cases, where we have calculated the replacement relations for "hard" inclusions from the pores and "soft" inclusions from absolutely rigid ones, the results have shown incorrect behavior. It should be noted that one may expect better results in the case of different convex polyhedra, for instance, superspheres, due to the fact that Trofimov et al. (2017b) have obtained the worst correspondence for tetrahedral inclusions.

To improve the results of applicability of the replacement relations, the so-called adjustment tensors were proposed; the components of these tensors were linearly dependent on the inhomogeneity shape parameter p (that is inversely proportional to the surface curvature of the inhomogeneity). Application of such tensors allowed us to adjust the results well only in the case of "soft" inclusions.

Overall, one may conclude that, for tetrahedron-like inclusions, the replacement relations work reasonably well only in the case of "soft" inclusions, i.e., which Young's modulus is lower that the matrix'. The error increases, as the inclusion shape becomes more concave, however, the behavior of this error with respect to the parameter p is close to linear, as the calculation of the adjustment tensors have shown.

Supplementary material

Supplementary material associated with this article can be found, in the online version, at doi:10.1016/j.ijsolstr.2019.02.020.

Appendix A

In this Appendix we give the calculations of the 5 independent constants of the transversally isotropic compliance contribution tensor **H** by the two considered numerical techniques: the FEM and the VIEM.

Tables A1–A5

Table A1
Component H_{1111} of the compliance contribution tensor calculated by the FEM and the VIEM.

	E^1/E^0							
p	∞ (rigid)	10	5	2	0.5	0.2	0.1	0 (void)
	H_{1111}^{FEM}							
−0.3	−5.505	−2.294	−1.623	−0.700	0.679	1.488	1.977	2.827
−0.25	−4.834	−2.262	−1.613	−0.699	0.679	1.484	1.968	2.802
−0.2	−4.333	−2.222	−1.599	−0.698	0.678	1.478	1.954	2.767
−0.15	−3.956	−2.180	−1.583	−0.696	0.677	1.471	1.938	2.723
−0.1	−3.661	−2.139	−1.568	−0.695	0.677	1.463	1.921	2.676
0	−2.954	−1.995	−1.511	−0.691	0.674	1.459	1.902	2.597
0.25	−2.642	−1.868	−1.424	−0.685	0.671	1.447	1.826	2.339
0.5	−2.321	−1.768	−1.386	−0.678	0.670	1.396	1.735	2.164
0.75	−2.129	−1.705	−1.372	−0.673	0.666	1.342	1.658	2.049
1	−2.030	−1.658	−1.346	−0.667	0.665	1.331	1.638	2.001
	H_{1111}^{VIEM}							
−0.3	−4.868	−2.197	−1.595	−0.692	0.690	1.517	2.021	2.913
−0.25	−4.365	−2.170	−1.586	−0.692	0.687	1.502	2.003	2.863
−0.2	−3.986	−2.159	−1.577	−0.691	0.684	1.487	1.966	2.808
−0.15	−3.837	−2.154	−1.573	−0.689	0.683	1.484	1.944	2.750
−0.1	−3.652	−2.111	−1.568	−0.687	0.682	1.480	1.927	2.692
0	−2.929	−1.981	−1.497	−0.685	0.681	1.473	1.917	2.621
0.25	−2.616	−1.876	−1.450	−0.681	0.675	1.423	1.810	2.391
0.5	−2.353	−1.780	−1.404	−0.675	0.670	1.383	1.727	2.196
0.75	−2.154	−1.700	−1.365	−0.670	0.667	1.353	1.668	2.064
1	−2.030	−1.658	−1.346	−0.667	0.665	1.331	1.638	2.002

Table A2
The same as in Table A1 for the component H_{3333}.

	E^1/E^0							
p	∞ (rigid)	10	5	2	0.5	0.2	0.1	0 (void)
	H^{FEM}_{3333}							
−0.3	−5.685	−2.412	−1.687	−0.712	0.668	1.440	1.900	2.699
−0.25	−4.972	−2.370	−1.673	−0.711	0.668	1.437	1.893	2.679
−0.2	−4.436	−2.318	−1.655	−0.709	0.667	1.433	1.883	2.650
−0.15	−4.033	−2.265	−1.635	−0.707	0.667	1.428	1.870	2.614
−0.1	−3.719	−2.213	−1.614	−0.705	0.667	1.422	1.856	2.574
0	−3.005	−2.051	−1.532	−0.696	0.666	1.421	1.840	2.544
0.25	−2.645	−1.899	−1.447	−0.687	0.666	1.414	1.792	2.287
0.5	−2.325	−1.784	−1.400	−0.678	0.665	1.382	1.716	2.137
0.75	−2.132	−1.711	−1.377	−0.674	0.664	1.337	1.651	2.041
1	−2.030	−1.658	−1.346	−0.667	0.665	1.331	1.637	2.002
	H^{VIEM}_{3333}							
−0.3	−4.987	−2.311	−1.624	−0.700	0.682	1.482	1.958	2.786
−0.25	−4.505	−2.276	−1.624	−0.700	0.678	1.464	1.933	2.743
−0.2	−4.066	−2.246	−1.620	−0.700	0.676	1.452	1.910	2.686
−0.15	−3.923	−2.235	−1.620	−0.698	0.675	1.449	1.890	2.663
−0.1	−3.698	−2.210	−1.605	−0.695	0.674	1.447	1.886	2.622
0	−2.984	−2.031	−1.530	−0.693	0.674	1.445	1.874	2.601
0.25	−2.634	−1.905	−1.462	−0.687	0.670	1.402	1.779	2.346
0.5	−2.365	−1.797	−1.414	−0.679	0.667	1.370	1.709	2.168
0.75	−2.160	−1.707	−1.370	−0.672	0.666	1.349	1.661	2.054
1	−2.030	−1.658	−1.347	−0.667	0.665	1.331	1.638	2.002

Table A3
The same as in Table A1 for the component H_{1122}.

	E^1/E^0							
p	∞ (rigid)	10	5	2	0.5	0.2	0.1	0 (void)
	H^{FEM}_{1122}							
−0.3	2.188	0.737	0.513	0.216	−0.195	−0.392	−0.480	−0.553
−0.25	1.898	0.730	0.511	0.216	−0.195	−0.390	−0.478	−0.550
−0.2	1.682	0.722	0.508	0.216	−0.195	−0.389	−0.474	−0.545
−0.15	1.520	0.712	0.505	0.215	−0.194	−0.387	−0.471	−0.540
−0.1	1.393	0.702	0.502	0.215	−0.194	−0.384	−0.466	−0.535
0	1.060	0.657	0.484	0.215	−0.193	−0.385	−0.459	−0.525
0.25	0.955	0.634	0.471	0.214	−0.192	−0.375	−0.445	−0.504
0.5	0.814	0.599	0.459	0.213	−0.191	−0.363	−0.428	−0.491
0.75	0.732	0.571	0.450	0.212	−0.189	−0.352	−0.416	−0.482
1	0.693	0.555	0.443	0.210	−0.188	−0.349	−0.412	−0.476
	H^{VIEM}_{1122}							
−0.3	1.930	0.718	0.504	0.215	−0.198	−0.403	−0.492	−0.570
−0.25	1.716	0.717	0.503	0.215	−0.197	−0.399	−0.486	−0.562
−0.2	1.539	0.713	0.501	0.215	−0.197	−0.394	−0.481	−0.555
−0.15	1.477	0.709	0.499	0.214	−0.196	−0.393	−0.480	−0.549
−0.1	1.389	0.697	0.494	0.213	−0.195	−0.391	−0.472	−0.541
0	1.051	0.652	0.480	0.213	−0.195	−0.388	−0.462	−0.526
0.25	0.941	0.625	0.471	0.212	−0.192	−0.374	−0.447	−0.510
0.5	0.830	0.595	0.459	0.211	−0.191	−0.363	−0.431	−0.500
0.75	0.745	0.568	0.447	0.211	−0.189	−0.356	−0.419	−0.486
1	0.692	0.555	0.443	0.210	−0.188	−0.349	−0.412	−0.476

Table A4
The same as in Table A1 for the component H_{1133}.

	E^1/E^0							
p	∞ (rigid)	10	5	2	0.5	0.2	0.1	0 (void)
	H^{FEM}_{1133}							
−0.3	2.370	0.857	0.578	0.229	−0.184	−0.343	−0.402	−0.423
−0.25	2.032	0.840	0.573	0.228	−0.184	−0.343	−0.401	−0.423
−0.2	1.780	0.821	0.566	0.227	−0.184	−0.342	−0.400	−0.424
−0.15	1.591	0.800	0.558	0.227	−0.184	−0.342	−0.400	−0.425
−0.1	1.445	0.780	0.550	0.226	−0.184	−0.342	−0.399	−0.426
0	1.096	0.710	0.520	0.221	−0.185	−0.344	−0.401	−0.430
0.25	0.957	0.671	0.500	0.214	−0.187	−0.345	−0.402	−0.444
0.5	0.821	0.617	0.474	0.211	−0.187	−0.348	−0.406	−0.458
0.75	0.738	0.579	0.456	0.209	−0.187	−0.350	−0.407	−0.469
1	0.693	0.555	0.443	0.210	−0.188	−0.349	−0.412	−0.476
	H^{VIEM}_{1133}							
−0.3	2.053	0.791	0.559	0.225	−0.189	−0.358	−0.420	−0.480
−0.25	1.783	0.789	0.556	0.224	−0.188	−0.356	−0.417	−0.470
−0.2	1.602	0.787	0.555	0.224	−0.188	−0.355	−0.416	−0.469
−0.15	1.531	0.785	0.554	0.224	−0.187	−0.354	−0.413	−0.466
−0.1	1.438	0.776	0.548	0.222	−0.187	−0.354	−0.412	−0.465
0	1.093	0.706	0.517	0.221	−0.187	−0.354	−0.411	−0.463
0.25	0.949	0.656	0.494	0.218	−0.187	−0.350	−0.410	−0.464
0.5	0.836	0.613	0.473	0.215	−0.187	−0.349	−0.409	−0.467
0.75	0.749	0.576	0.454	0.212	−0.187	−0.347	−0.410	−0.472
1	0.692	0.555	0.443	0.210	−0.188	−0.349	−0.412	−0.476

Table A5
The same as in Table A1 for the component H_{1313}.

	E^1/E^0							
p	∞ (rigid)	10	5	2	0.5	0.2	0.1	0 (void)
	H^{FEM}_{1313}							
−0.3	−3.846	−1.394	−1.002	−0.445	0.448	0.989	1.307	1.820
−0.25	−3.366	−1.383	−0.999	−0.445	0.448	0.986	1.300	1.804
−0.2	−3.007	−1.370	−0.994	−0.445	0.447	0.981	1.290	1.780
−0.15	−2.738	−1.355	−0.989	−0.444	0.447	0.975	1.277	1.750
−0.1	−2.527	−1.340	−0.984	−0.444	0.446	0.968	1.263	1.717
0	−2.022	−1.258	−0.950	−0.444	0.445	0.954	1.248	1.670
0.25	−1.792	−1.222	−0.928	−0.442	0.440	0.931	1.169	1.485
0.5	−1.554	−1.168	−0.913	−0.441	0.434	0.889	1.099	1.363
0.75	−1.420	−1.128	−0.903	−0.440	0.429	0.855	1.048	1.282
1	−1.362	−1.106	−0.890	−0.438	0.427	0.840	1.026	1.239
	H^{VIEM}_{1313}							
−0.3	−3.386	−1.370	−0.991	−0.446	0.454	1.008	1.344	1.882
−0.25	−3.049	−1.367	−0.988	−0.445	0.452	0.996	1.321	1.847
−0.2	−2.761	−1.360	−0.984	−0.444	0.451	0.986	1.300	1.807
−0.15	−2.671	−1.352	−0.980	−0.443	0.449	0.982	1.280	1.771
−0.1	−2.507	−1.338	−0.973	−0.442	0.448	0.977	1.265	1.735
0	−1.988	−1.257	−0.949	−0.440	0.447	0.972	1.261	1.715
0.25	−1.798	−1.216	−0.935	−0.440	0.440	0.926	1.172	1.524
0.5	−1.604	−1.168	−0.916	−0.439	0.435	0.890	1.104	1.385
0.75	−1.452	−1.125	−0.899	−0.439	0.430	0.862	1.055	1.293
1	−1.361	−1.106	−0.890	−0.438	0.427	0.840	1.026	1.239

Appendix B

In this Appendix we give the calculations of the four remaining (besides H_{1111}) independent constants of the transversally isotropic compliance contribution tensor **H** by the replacement relation given in Section 4. We consider two calculation variants: we obtain the tensor **H** considering the inhomogeneity "B" is either rigid or represents a pore. For the calculations the results obtained by the VIEM are taken.

Tables B1–B4

Table B1
Component H_{3333} of the compliance contribution tensor calculated by the replacement relation from an inhomogeneity "B" that is either absolutely rigid or represents a pore.

	E^A/E^0							
p	∞ (rigid)	10	5	2	0.5	0.2	0.1	0 (void)
	H^{RRigid}_{3333}							
−0.3	−4.987	−3.177	−2.188	−0.824	0.563	0.980	1.137	1.303
−0.25	−4.505	−2.984	−2.099	−0.812	0.568	0.993	1.154	1.325
−0.2	−4.066	−2.785	−1.999	−0.797	0.576	1.018	1.188	1.371
−0.15	−3.923	−2.719	−1.965	−0.791	0.579	1.026	1.199	1.385
−0.1	−3.698	−2.610	−1.907	−0.782	0.584	1.043	1.222	1.415
0	−2.984	−2.238	−1.704	−0.746	0.604	1.108	1.311	1.536
0.25	−2.634	−2.037	−1.585	−0.723	0.621	1.165	1.392	1.648
0.5	−2.365	−1.873	−1.484	−0.701	0.637	1.224	1.477	1.769
0.75	−2.160	−1.743	−1.402	−0.683	0.653	1.284	1.565	1.897
1	−2.030	−1.658	−1.347	−0.669	0.665	1.330	1.633	2.002
	H^{RPore}_{3333}							
−0.3	−1.604	−1.362	−1.145	−0.615	0.730	1.624	2.111	2.786
−0.25	−1.621	−1.374	−1.153	−0.618	0.727	1.609	2.085	2.743
−0.2	−1.640	−1.388	−1.163	−0.621	0.723	1.590	2.053	2.686
−0.15	−1.651	−1.395	−1.168	−0.622	0.721	1.582	2.040	2.663
−0.1	−1.666	−1.407	−1.176	−0.624	0.718	1.568	2.016	2.622
0	−1.677	−1.414	−1.181	−0.625	0.717	1.561	2.004	2.601
0.25	−1.747	−1.463	−1.215	−0.635	0.704	1.500	1.903	2.346
0.5	−1.901	−1.570	−1.288	−0.654	0.681	1.400	1.743	2.168
0.75	−1.986	−1.628	−1.327	−0.664	0.671	1.354	1.671	2.054
1	−2.030	−1.658	−1.347	−0.669	0.665	1.330	1.633	2.002

Table B2
The same as in Table B1 for the component H_{1122}.

	E^A/E^0							
p	∞ (rigid)	10	5	2	0.5	0.2	0.1	0 (void)
	H^{RRigid}_{1122}							
−0.3	1.930	1.184	0.786	0.271	−0.154	−0.243	−0.270	−0.294
−0.25	1.716	1.095	0.744	0.265	−0.156	−0.251	−0.280	−0.307
−0.2	1.539	1.016	0.705	0.260	−0.159	−0.257	−0.288	−0.316
−0.15	1.477	0.988	0.691	0.258	−0.159	−0.259	−0.290	−0.319
−0.1	1.389	0.945	0.669	0.254	−0.161	−0.263	−0.296	−0.327
0	1.051	0.769	0.573	0.238	−0.170	−0.291	−0.333	−0.375
0.25	0.941	0.708	0.538	0.231	−0.173	−0.300	−0.344	−0.387
0.5	0.830	0.642	0.498	0.223	−0.178	−0.315	−0.365	−0.413
0.75	0.745	0.589	0.465	0.216	−0.184	−0.334	−0.390	−0.447
1	0.692	0.555	0.443	0.211	−0.188	−0.348	−0.411	−0.476
	H^{RPore}_{1122}							
−0.3	0.510	0.431	0.360	0.190	−0.208	−0.419	−0.504	−0.570
−0.25	0.516	0.435	0.363	0.191	−0.207	−0.415	−0.497	−0.562
−0.2	0.522	0.440	0.366	0.192	−0.206	−0.410	−0.491	−0.555
−0.15	0.530	0.445	0.370	0.193	−0.205	−0.406	−0.485	−0.549
−0.1	0.538	0.451	0.374	0.194	−0.203	−0.400	−0.477	−0.541
0	0.552	0.460	0.380	0.196	−0.201	−0.393	−0.466	−0.526
0.25	0.566	0.470	0.387	0.197	−0.200	−0.390	−0.466	−0.520
0.5	0.627	0.512	0.415	0.205	−0.193	−0.365	−0.433	−0.500
0.75	0.667	0.538	0.432	0.209	−0.190	−0.355	−0.420	−0.486
1	0.692	0.555	0.443	0.211	−0.188	−0.348	−0.411	−0.476

Table B3
The same as in Table B1 for the component H_{1133}.

	E^A/E^0							
p	∞ (rigid)	10	5	2	0.5	0.2	0.1	0 (void)
	H^{RRigid}_{1133}							
−0.3	2.053	1.234	0.809	0.274	−0.152	−0.239	−0.265	−0.287
−0.25	1.783	1.122	0.756	0.267	−0.156	−0.250	−0.279	−0.306
−0.2	1.602	1.045	0.719	0.262	−0.158	−0.254	−0.284	−0.311
−0.15	1.531	1.012	0.703	0.259	−0.159	−0.257	−0.287	−0.315
−0.1	1.438	0.969	0.682	0.256	−0.160	−0.260	−0.292	−0.321
0	1.093	0.792	0.586	0.240	−0.169	−0.286	−0.327	−0.366
0.25	0.949	0.713	0.540	0.232	−0.173	−0.299	−0.342	−0.385
0.5	0.836	0.646	0.500	0.224	−0.178	−0.314	−0.363	−0.411
0.75	0.749	0.591	0.466	0.217	−0.183	−0.333	−0.389	−0.445
1	0.692	0.555	0.443	0.211	−0.188	−0.348	−0.411	−0.476
	H^{RPore}_{1133}							
−0.3	0.545	0.456	0.378	0.195	−0.201	−0.386	−0.449	−0.480
−0.25	0.553	0.462	0.382	0.196	−0.200	−0.381	−0.441	−0.470
−0.2	0.560	0.467	0.385	0.197	−0.199	−0.377	−0.437	−0.469
−0.15	0.566	0.471	0.388	0.198	−0.198	−0.375	−0.434	−0.466
−0.1	0.572	0.475	0.391	0.199	−0.197	−0.372	−0.431	−0.465
0	0.578	0.479	0.394	0.200	−0.196	−0.369	−0.427	−0.463
0.25	0.601	0.495	0.404	0.202	−0.194	−0.365	−0.426	−0.464
0.5	0.656	0.532	0.428	0.208	−0.190	−0.351	−0.410	−0.467
0.75	0.682	0.548	0.439	0.210	−0.188	−0.348	−0.410	−0.472
1	0.692	0.555	0.443	0.211	−0.188	−0.348	−0.411	−0.476

Table B4
The same as in Table B1 for the component H_{1313}.

	E^A/E^0							
p	∞ (rigid)	10	5	2	0.5	0.2	0.1	0 (void)
	H^{RRigid}_{1313}							
−0.3	−3.386	−2.152	−1.474	−0.546	0.359	0.614	0.707	0.803
−0.25	−3.049	−2.010	−1.406	−0.536	0.364	0.626	0.723	0.824
−0.2	−2.761	−1.881	−1.342	−0.527	0.368	0.640	0.742	0.848
−0.15	−2.671	−1.839	−1.320	−0.523	0.370	0.645	0.748	0.857
−0.1	−2.507	−1.760	−1.279	−0.517	0.373	0.655	0.762	0.875
0	−1.988	−1.520	−1.147	−0.494	0.386	0.697	0.818	0.950
0.25	−1.798	−1.378	−1.065	−0.478	0.397	0.731	0.866	1.015
0.5	−1.604	−1.261	−0.993	−0.463	0.407	0.769	0.920	1.089
0.75	−1.452	−1.165	−0.933	−0.449	0.418	0.809	0.978	1.173
1	−1.361	−1.107	−0.895	−0.440	0.426	0.839	1.022	1.239
	H^{RPore}_{1313}							
−0.3	−0.992	−0.849	−0.719	−0.393	0.483	1.093	1.427	1.882
−0.25	−1.002	−0.857	−0.724	−0.394	0.481	1.081	1.407	1.847
−0.2	−1.014	−0.864	−0.730	−0.396	0.478	1.068	1.383	1.807
−0.15	−1.026	−0.874	−0.736	−0.398	0.476	1.055	1.362	1.771
−0.1	−1.038	−0.883	−0.743	−0.400	0.473	1.042	1.341	1.735
0	−1.045	−0.888	−0.746	−0.401	0.472	1.035	1.329	1.715
0.25	−1.105	−0.931	−0.776	−0.409	0.460	0.982	1.242	1.524
0.5	−1.221	−1.012	−0.832	−0.424	0.443	0.905	1.122	1.385
0.75	−1.303	−1.067	−0.869	−0.434	0.433	0.864	1.060	1.293
1	−1.361	−1.107	−0.895	−0.440	0.426	0.839	1.022	1.239

Appendix C

In this Appendix we give the calculations of the four remaining (besides 1111) independent constants of the transversally isotropic tensors $\mathbf{H}^{RRigid*}$ and $\mathbf{H}^{RPore*}$.

Tables C1–C4

Table C1
Calculation of the component H_{3333} of the compliance contribution tensor calculated by the replacement relation combined with the corresponding adjustment tensor.

	E^A/E^0							
p	∞ (rigid)	10	5	2	0.5	0.2	0.1	0 (void)
	$H_{3333}^{RRigid*}$				H_{3333}^{RPore*}			
−0.3	−4.987	−2.588	−1.786	−0.675	0.671	1.492	1.938	2.786
−0.25	−4.505	−2.458	−1.732	−0.672	0.670	1.483	1.921	2.743
−0.2	−4.066	−2.317	−1.665	−0.666	0.669	1.471	1.898	2.686
−0.15	−3.923	−2.285	−1.653	−0.667	0.670	1.469	1.893	2.663
−0.1	−3.698	−2.214	−1.620	−0.666	0.669	1.461	1.878	2.622
0	−2.984	−1.937	−1.476	−0.647	0.673	1.465	1.880	2.601
0.25	−2.634	−1.845	−1.437	−0.656	0.672	1.432	1.817	2.346
0.5	−2.365	−1.772	−1.404	−0.664	0.662	1.360	1.693	2.168
0.75	−2.160	−1.719	−1.383	−0.674	0.663	1.338	1.651	2.054
1	−2.030	−1.658	−1.347	−0.667	0.665	1.331	1.638	2.002

Table C2
The same as in Table C1 for the component H_{1122}.

	E^A/E^0							
p	∞ (rigid)	10	5	2	0.5	0.2	0.1	0 (void)
	$H_{1122}^{RRigid*}$				H_{1122}^{RPore*}			
−0.3	2.188	0.870	0.572	0.193	−0.199	−0.404	−0.489	−0.553
−0.25	1.898	0.815	0.549	0.192	−0.199	−0.401	−0.483	−0.550
−0.2	1.682	0.766	0.528	0.191	−0.198	−0.397	−0.477	−0.545
−0.15	1.520	0.756	0.525	0.193	−0.197	−0.393	−0.472	−0.540
−0.1	1.393	0.733	0.516	0.193	−0.196	−0.388	−0.465	−0.535
0	1.060	0.611	0.453	0.186	−0.195	−0.382	−0.455	−0.525
0.25	0.955	0.605	0.458	0.196	−0.195	−0.382	−0.458	−0.504
0.5	0.814	0.587	0.455	0.203	−0.190	−0.360	−0.428	−0.491
0.75	0.732	0.574	0.453	0.210	−0.189	−0.353	−0.418	−0.482
1	0.693	0.555	0.443	0.210	−0.188	−0.349	−0.412	−0.476

Table C3
The same as in Table C1 for the component H_{1133}.

	E^A/E^0							
p	∞ (rigid)	10	5	2	0.5	0.2	0.1	0 (void)
	$H_{1133}^{RRigid*}$				H_{1133}^{RPore*}			
−0.3	2.370	0.967	0.630	0.210	−0.188	−0.362	−0.423	−0.423
−0.25	2.032	0.886	0.594	0.207	−0.187	−0.359	−0.417	−0.423
−0.2	1.780	0.835	0.572	0.206	−0.187	−0.356	−0.414	−0.424
−0.15	1.591	0.818	0.566	0.206	−0.186	−0.355	−0.413	−0.425
−0.1	1.445	0.793	0.555	0.206	−0.186	−0.353	−0.411	−0.426
0	1.096	0.660	0.487	0.198	−0.186	−0.352	−0.409	−0.430
0.25	0.957	0.630	0.476	0.204	−0.187	−0.353	−0.413	−0.444
0.5	0.821	0.603	0.466	0.209	−0.186	−0.344	−0.403	−0.458
0.75	0.738	0.582	0.459	0.214	−0.187	−0.346	−0.408	−0.469
1	0.693	0.555	0.443	0.210	−0.188	−0.349	−0.412	−0.476

Table C4
The same as in Table C1 for the component H_{1313}.

	E^A/E^0							
p	∞ (rigid)	10	5	2	0.5	0.2	0.1	0 (void)
	$H_{1313}^{RRigid*}$				H_{1313}^{RPore*}			
−0.3	−3.386	−1.603	−1.098	−0.407	0.449	1.016	1.327	1.882
−0.25	−3.049	−1.519	−1.063	−0.405	0.449	1.008	1.312	1.847
−0.2	−2.761	−1.442	−1.029	−0.404	0.447	0.999	1.294	1.807
−0.15	−2.671	−1.429	−1.026	−0.407	0.447	0.990	1.278	1.771
−0.1	−2.507	−1.387	−1.008	−0.407	0.445	0.981	1.262	1.735
0	−1.988	−1.231	−0.929	−0.400	0.447	0.980	1.259	1.715
0.25	−1.798	−1.190	−0.920	−0.413	0.442	0.944	1.194	1.524
0.5	−1.604	−1.157	−0.911	−0.425	0.432	0.883	1.095	1.385
0.75	−1.452	−1.131	−0.906	−0.436	0.429	0.856	1.050	1.293
1	−1.361	−1.106	−0.890	−0.438	0.427	0.840	1.026	1.239

References

Argatov, I., Sevostianov, I., 2011. Rigid toroidal inhomogeneity in an elastic medium. Int. J. Eng. Sci. 49, 61–74. doi:10.1016/j.ijengsci.2010.06.023.

Benveniste, Y., 1987. A new approach to the application of Mori–Tanaka's theory in composite materials. Mech. Mater. 6, 147–157. doi:10.1016/0167-6636(87)90005-6.

Chen, F., Sevostianov, I., Giraud, A., Grgic, D., 2017. Accuracy of the replacement relations for materials with non-ellipsoidal inhomogeneities. Int. J. Solids Struct. 104–105, 73–80. doi:10.1016/j.ijsolstr.2016.10.023.

Chen, F., Sevostianov, I., Giraud, A., Grgic, D., 2015. Evaluation of the effective elastic and conductive properties of a material containing concave pores. Int. J. Eng. Sci. 97, 60–68. doi:10.1016/j.ijengsci.2015.08.012.

Ciz, R., Shapiro, S.A., 2007. Generalization of Gassmann equations for porous media saturated with a solid material. Geophysics 72, A75–A79.

Drach, B., Drach, A., Tsukrov, I., 2014. Prediction of the effective elastic moduli of materials with irregularly-shaped pores based on the pore projected areas. Int. J. Solids Struct. 51, 2687–2695. doi:10.1016/j.ijsolstr.2014.03.042.

Drach, B., Tsukrov, I., Gross, T.S., Dietrich, S., Weidenmann, K., Piat, R., Böhlke, T., 2011. Numerical modeling of carbon/carbon composites with nanotextured matrix and 3D pores of irregular shapes. Int. J. Solids Struct. 48, 2447–2457. doi:10.1016/j.ijsolstr.2011.04.021.

Eshelby, J.D., 1961. Elastic inclusions and inhomogeneities. Prog. Solid Mech. 2, 89–140.

Eshelby, J.D., 1957. The determination of the elastic field of an ellipsoidal inclusion, and related problems. Proc. R. Soc. A Math. Phys. Eng. Sci. 241, 376–396. doi:10.1098/rspa.1957.0133.

Garboczi, E.J., Douglas, J.F., 2012. Elastic moduli of composites containing a low concentration of complex-shaped particles having a general property contrast with the matrix. Mech. Mater. 51, 53–65. doi:10.1016/j.mechmat.2012.03.009.

Gassman, F., 1951. Über die Elastizität poröser Medien. Vierteljahrsschrift der Naturforschenden Gesellschaft Zürich 96, 1–23.

Golub, G.H., Van Loan, C.F., 1996. Matrix Computations, 3rd Ed. Matrix Computations doi:10.1103/PhysRevB.34.5414.

Horii, H., Nemat-Nasser, S., 1983. Overall moduli of solids with microcracks: load-induced anisotropy. J. Mech. Phys. Solids. doi:10.1016/0022-5096(83)90048-0.

Jaeger, L.C., Cook, N.G.W., Zimmerman, R.W., 2007. Fundamentals of Rock Mechanics, 4th ed. Blackwell Publishing Ltd, Oxford.

Kachanov, M., Sevostianov, I., 2018. Micromechanics of Materials, with Applications. Springer International Publishing. doi:10.1007/978-3-319-76204-3.

Kachanov, M., Tsukrov, I., Shafiro, B., 1994. Effective moduli of solids with cavities of various shapes. Appl. Mech. Rev. 47, S151. doi:10.1115/1.3122810.

Kanaun, S., 2011. An efficient numerical method for calculation of elastic and thermo-elastic fields in a homogeneous medium with several heterogeneous inclusions. World J. Mech. 1, 31–43. doi:10.4236/wjm.2011.12005.

Kanaun, S., 2009. Fast calculation of elastic fields in a homogeneous medium with isolated heterogeneous inclusions. Int. J. Multiscale Comput. Eng. 7, 263–276. doi:10.1615/IntJMultCompEng.v7.i4.30.

Kanaun, S., 1981. Elastic problem for 3D-anisotropic medium with a crack. Appl. Math. Mech. 45, 361–370.

Kanaun, S., Levin, V., 2008. Self-consistent Methods For Composites I. Springer, Dordrecht.

Kanaun, S., Markov, A., Babaii, S., 2013. An efficient numerical method for the solution of the second boundary value problem of elasticity for 3D-bodies with cracks. Int. J. Fract. 183, 169–186. doi:10.1007/s10704-013-9885-5.

Kanaun, S., Pervago, E., 2011. Combining self-consistent and numerical methods for the calculation of elastic fields and effective properties of 3D-matrix composites with periodic and random microstructures. Int. J. Eng. Sci. 49, 420–442. doi:10.1016/j.ijengsci.2011.01.001.

Krasnitskii, S., Trofimov, A., Radi, E., Sevestianov, I., 2018. Effect of a rigid toroidal inhomogeneity on the elastic properties of a composite. Math. Mech. Solids. doi:10.1177/1081286518773806.

Kunin, I., 1983. The Theory of Elastic Media with Microstructure II. Springer, Berlin, Heidelberg.
Li, D., He, X., Su, M., Zhao, Y., Li, J., Huang, T., Liu, H., 2017. One-pot synthesis of hierarchical concave tetrapod Pd nanocrystals and their electrocatalytic properties. RSC Adv. 7, 37938–37942. doi:10.1039/C7RA05505F.
Markov, A., Kanaun, S., 2018. An efficient numerical method for quasi-static crack propagation in heterogeneous media. Int. J. Fract. 212, 1–47. doi:10.1007/s10704-018-0284-9.
Markov, A., Kanaun, S., 2017. Interactions of cracks and inclusions in homogeneous elastic media. Int. J. Fract. 206, 35–48. doi:10.1007/s10704-017-0199-x.
Mavko, G., Mukerji, T., Dvorkin, J., 2009. The Rock Physics Handbook: Tools for Seismic Analysis in Porous Media. Cambridge University Press.
Maz'ya, V., Schmidt, G., 2007. Approximate Approximations. AMS Mathematical Surveys and Monographs, Providence.
Mori, T., Tanaka, K., 1973. Average stress in matrix and average elastic energy of materials with misfitting inclusions. Acta Metall. 21, 571–574. doi:10.1016/0001-6160(73)90064-3.
Park, K.H., Jang, K., Kim, H.J., Son, S.U., 2007. Near-monodisperse tetrahedral rhodium nanoparticles on charcoal: the shape-dependent catalytic hydrogenation of arenes. Angew. Chemie Int. Ed. 46, 1152–1155. doi:10.1002/anie.200603961.
Popov, E., Trofimov, A., Goncharov, A., Abaimov, S., Chekhonin, E., Popov, Y., Sevostianov, I., 2018. Technique of rock thermal conductivity evaluation on core cuttings and non-consolidated rocks. Int. J. Rock Mech. Min. Sci. 108, 15–22. doi:10.1016/j.ijrmms.2018.05.005.
Radi, E., Sevostianov, I., 2016. Toroidal insulating inhomogeneity in an infinite space and related problems. Proc. R. Soc. A Math. Phys. Eng. Sci. 472, 20150781. doi:10.1098/rspa.2015.0781.
Rasool, A., Böhm, H.J., 2012. Effects of particle shape on the macroscopic and microscopic linear behaviors of particle reinforced composites. Int. J. Eng. Sci. 58, 21–34. doi:10.1016/j.ijengsci.2012.03.022.
Saxena, N., Mavko, G., 2014. Exact equations for fluid and solid substitution. Geophysics 79, L21–L32. doi:10.1190/geo2013-0187.1.
Sevostianov, I., Abaimov, S.G., Trofimov, A., 2018. Replacement relations for thermal conductivities of heterogeneous materials having different matrices. Mech. Mater. 121, 50–56. doi:10.1016/j.mechmat.2018.03.003.
Sevostianov, I., Chen, F., Giraud, A., Grgic, D., 2016. Compliance and resistivity contribution tensors of axisymmetric concave pores. Int. J. Eng. Sci. 101, 14–28. doi:10.1016/j.ijengsci.2015.12.005.
Sevostianov, I., Giraud, A., 2013. Generalization of Maxwell homogenization scheme for elastic material containing inhomogeneities of diverse shape. Int. J. Eng. Sci. 64, 23–36. doi:10.1016/j.ijengsci.2012.12.004.
Sevostianov, I., Giraud, A., 2012. On the compliance contribution tensor for a concave superspherical pore. Int. J. Fract. 177, 199–206. doi:10.1007/s10704-012-9754-7.
Sevostianov, I., Kachanov, M., 2007. Relations between compliances of inhomogeneities having the same shape but different elastic constants. Int. J. Eng. Sci. 45, 797–806. doi:10.1016/j.ijengsci.2007.05.004.
Sevostianov, I., Kachanov, M., 2002. On elastic compliances of irregularly shaped cracks. Int. J. Fract. 114, 245–257. doi:10.1023/A:1015534127172.
Sevostianov, I., Kachanov, M., 2001. Elastic compliance of an annular crack. Int. J. Fract. 110, 51–54. doi:10.1023/A:1012283303397.
Sevostianov, I., Kachanov, M., 1999. Compliance tensors of ellipsoidal inclusions. Int. J. Fract. 96, 3–7. doi:10.1023/A:1018712913071.
Sevostianov, I., Kachanov, M., Zohdi, T., 2008. On computation of the compliance and stiffness contribution tensors of non ellipsoidal inhomogeneities. Int. J. Solids Struct. 45, 4375–4383. doi:10.1016/j.ijsolstr.2008.03.020.
Traxl, R., Lackner, R., 2018. Consideration of arbitrary inclusion shapes in the framework of isotropic continuum micromechanics: the replacement Eshelby tensor approach. Mech. Mater. 126, 126–139. doi:10.1016/j.mechmat.2018.08.010.
Trofimov, A., Abaimov, S., Akhatov, I., Sevostianov, I., 2017a. Effect of elastic contrast on the contribution of helical fibers into overall stiffness of a composites. Int. J. Eng. Sci. 120, 31–50. doi:10.1016/j.ijengsci.2017.06.014.
Trofimov, A., Abaimov, S., Sevostianov, I., 2018a. Inverse homogenization problem: evaluation of elastic and electrical (thermal) properties of composite constituents. Int. J. Eng. Sci. 129, 34–46. doi:10.1016/j.ijengsci.2018.04.001.
Trofimov, A., Drach, B., Sevostianov, I., 2017b. Effective elastic properties of composites with particles of polyhedral shapes. Int. J. Solids Struct. 120, 157–170. doi:10.1016/j.ijsolstr.2017.04.037.
Trofimov, A., Markov, A., Abaimov, S.G., Akhatov, I., Sevostianov, I., 2018b. Overall elastic properties of a material containing inhomogeneities of concave shape. Int. J. Eng. Sci. 132, 30–44. doi:10.1016/j.ijengsci.2018.07.004.
Trofimov, A., Sevostianov, I., 2017. The effect of waviness of a helical inhomogeneity on its stiffness- and conductivity contribution tensors. Int. J. Eng. Sci. 116, 145–154. doi:10.1016/j.ijengsci.2017.02.008.
Wark, D.A., Williams, C.A., Watson, E.B., Price, J.D., 2003. Reassessment of pore shapes in microstructurally equilibrated rocks, with implications for permeability of the upper mantle. J. Geophys. Res. Solid Earth 108. doi:10.1029/2001JB001575.